CHAPTER 5

RESULTS AND DISCUSSION

Chapter 5
Result and Discussion

5.1. **Batch Study**:

5.1.1. **Effect of Solution pH:**

Figure (5.1) represents the effect of initial pH on the %removal of Cr(VI) by Diaion SA20A resin. It is well seen that the sorption of Cr(VI) increases from 59.5 to 65 with the increase of pH from 2 to 4.28 . Beyond pH=4.28 there is a decrease in %Cr(VI) removal with further increase in pH to 6.

Thus optimum pH of 4.28 (pH of the solution) was chosen for further experiments. It should be noted that the chromate in solution may be found in various species such as H_2CrO_4, $HCrO_4^-$and $Cr_2O_7^{-2}$, which depend on the pH of the solution.

In the pH range from 0 to 6.5 $HCrO_4^-$ and $Cr_2O_7^{-2}$ are predominant, whereas at pH>6.5 only CrO_4^{-2} ion exist in the solution. [6, 28]

At very low pH values, the surface of the resin would be surrounded by the H^+ ions which enhance Cr(VI) interaction with binding sites of the resin by greater attractive force. [20, 21]

At pH>4.28, the decrease of %Cr(VI) removal can likely be ascribed to the decrease of $HCrO_4^-$ ion concentration and the effect of competitive binding between CrO_4^{2-} and OH^- for the binding sites on the surface of the resin.[86]

The present result is in agreement with previous studies. [34,45,55,63,64]

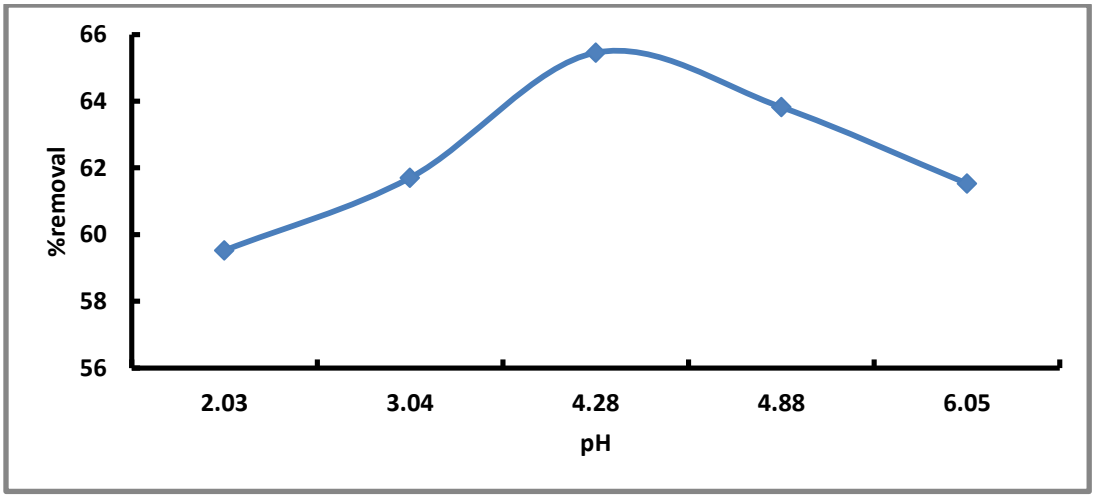

Figure 5-1 Effect of pH on the % removal of Cr(VI) by Diaion SA20A(conditions: C_o 200ppm; amount of resin, 5 g; temperature, 25±2 ◦C; stirring rate 350 rpm; t, 40 min)

5.1.2. **Effect of Contact Time:**

The effect of contact time on the % removal of Cr(VI) at different initial Cr(VI) concentrations is shown in Figure(5.2).

It is well noted that as contact time increases % Cr(VI) removal increases until a plateau is reached at about 40 minutes, it may concluded that at 40 minutes , equilibrium has been established between solute conc. in solid and its conc. in solution.

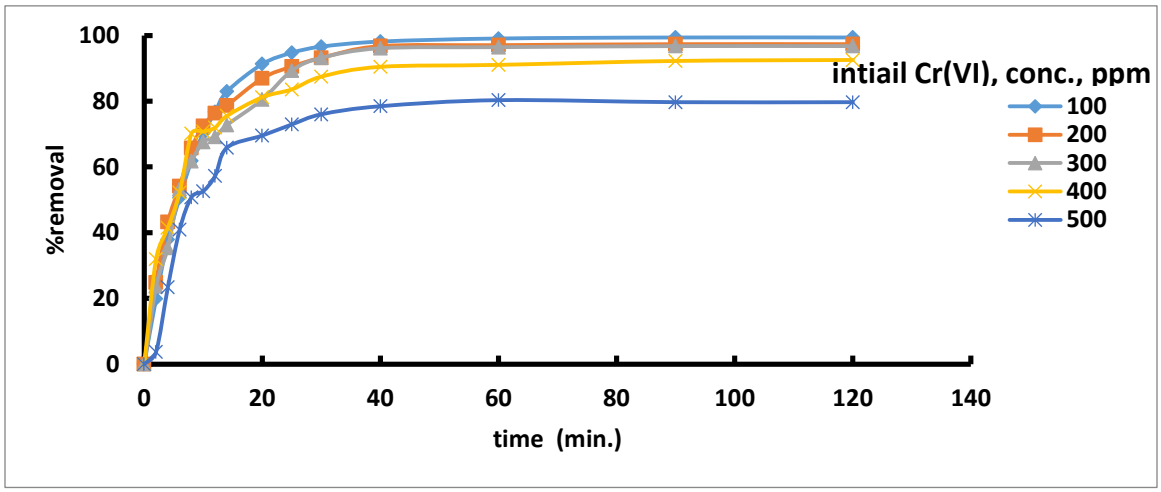

Figure 5-2 Effect of contact time on the %removal of Cr(VI) Diaion SA20A resin(amount of resin 5 g; temperature, 25±2 ˚C; stirring rate 350 rpm; initial pH 4.28)

5.1.3. **Effect of Initial Cr^{+6} Concentration:**

Figure (5.3) shows the effect of initial Cr(VI) concentrations on % removal. It is well seen that % removal of Cr(VI) decreases from 99.3 to 79.69% as the initial Cr(VI) increases from 100 ppm to 500 ppm. The present trend is in agreement with previous studies. [18,28]

It should be indicated that as the initial concentration of Cr(VI) ions increases for a constant resin weight the ratio of the exchange sites available to Cr(VI) ions decreases.

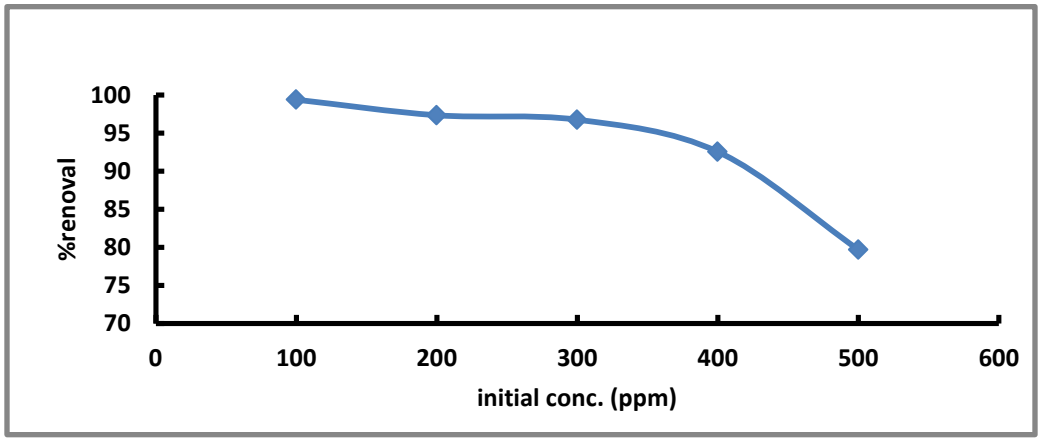

Figure 5-3 Effect of initial concentration on % removal of Cr(VI).(Initial pH of 4.28; Contact time of 120 min; amount of resin 5 g; and Temperature of 25±2°C & 350 rpm.)

5.1.4. **Effect of rpm:**

Figure (5.4) shows the effect of rpm on % Cr(VI) removal. It is well obvious that the increase of rpm from 350 to 600 increases %Cr(VI) removal from 54.84 to 70.27 % . As the rpm increases, the degree of mixing and turbulence increase, with a consequence decrease of both the hydrodynamic boundary layer and the concentration boundary layer thickness. The film resistance around each resin particle decreases and mass transfer rate increases. The present trend is in agreement with previous studies. [28]

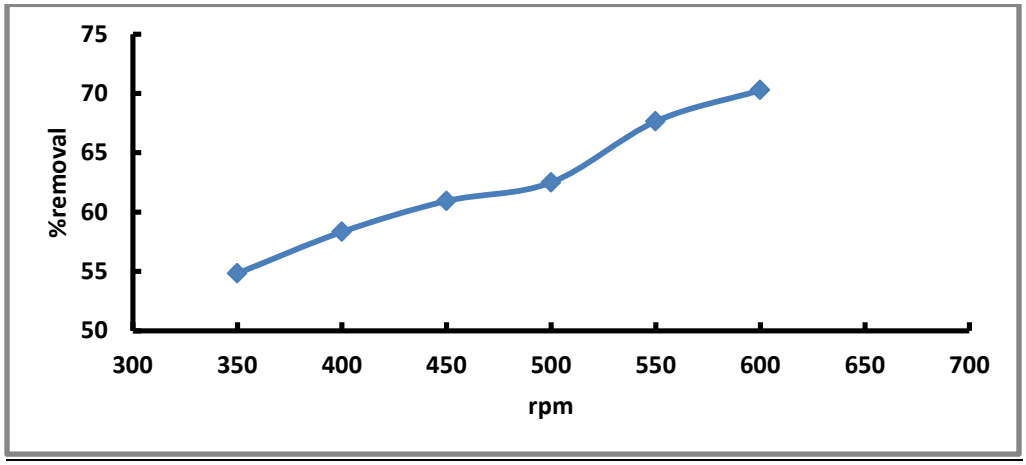

Figure 5-4 Effect of rpm on % Cr(VI) removal.(pH of 4.28; Contact time of 40 min; amount of resin 5 g; and Temp. 25±2 ^{o}C; C_o = 500ppm.)

5.1.5. **Effect of the Amount of Resin:**

Figure (5.5) shows the effect of the amount of resin on % Cr(VI) removal. It is well clear that as the amount of resin increases % Cr(VI) removal increases considerably. It is well known that the ratio of the number of available exchange sites to the number of Cr(VI) ions at fixed Cr(VI) concentration increases with the increase of the amount of resin and this results in an increase in %Cr(VI) removal. [28]

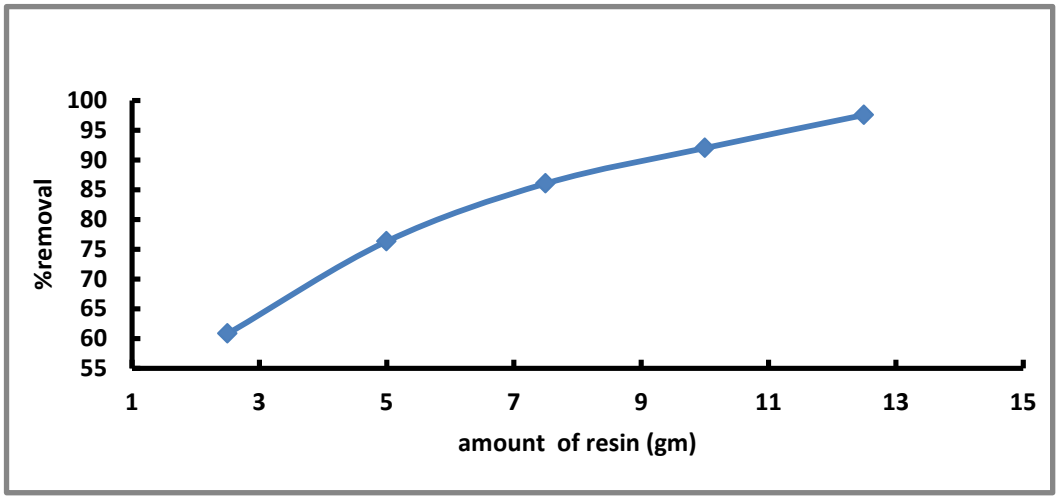

Figure 5-5 Effect of resin amount on % removal of Cr(VI).(Initial pH of 4.28; contact time 120 min; temperature of 25±2 ^{o}C; C_o = 200ppm & 350 rpm.)

5.1.6. **Effect of Temperature:**

The effect of temperature on the % removal of Cr(VI) by Diaion SA20A is shown in figure (5.6). It can be noticed that as temperature increases from 25^{o}C to 40^{o}C, % Cr(VI) removal increases from 54.83 to 80 . The increase of % Cr(VI) removal with temperature may be attributed to that as temperature increases, the viscosity of the solution decreases with a consequence increase of chromate diffusivity according to Stokes-Einstein equation.[22]

$$D\mu/T = \text{constant} \qquad (5.1)$$

The present results are in agreement with other investigators.[1,42,63]

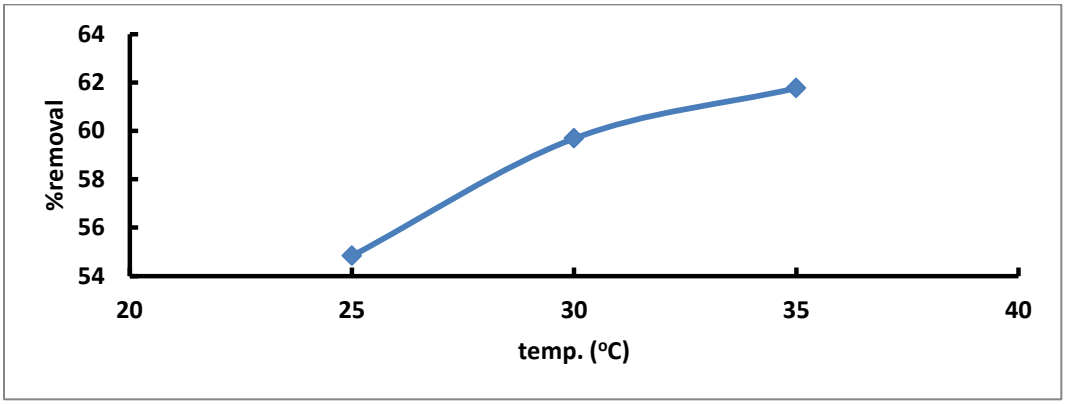

Figure 5-6 Effect of temperature on % Cr(VI) removal .(pH 4.28; Contact time 40 min; amount of resin 5 g;350 rpm &C_o = 500ppm .)

5.1.7. **Determination of the ion exchange Capacity:**

The amount of adsorption at time t, q_t (mg/g) was calculated by:

$$q_t = \frac{(C_o - C_t)V}{W} \qquad (5.2)$$

Where:

q_t (mg/g) = adsorption capacity at time (t), C_o (ppm) =initial concentration of Cr(VI) in the solution, C_t (ppm) = concentration of Cr(VI) at time (t), V (L) = volume of the waste water and W (g) = weight of the resin.

Figure (5.7) shows a plot of adsorption capacity versus time at different initial Cr(VI) concentrations.

It can be seen that as time increases the ion exchange capacity increases until a plateau is reached at about 40 minutes, it may concluded that at 40 minutes , equilibrium has been established between solute conc. in solid and its conc. in solution.

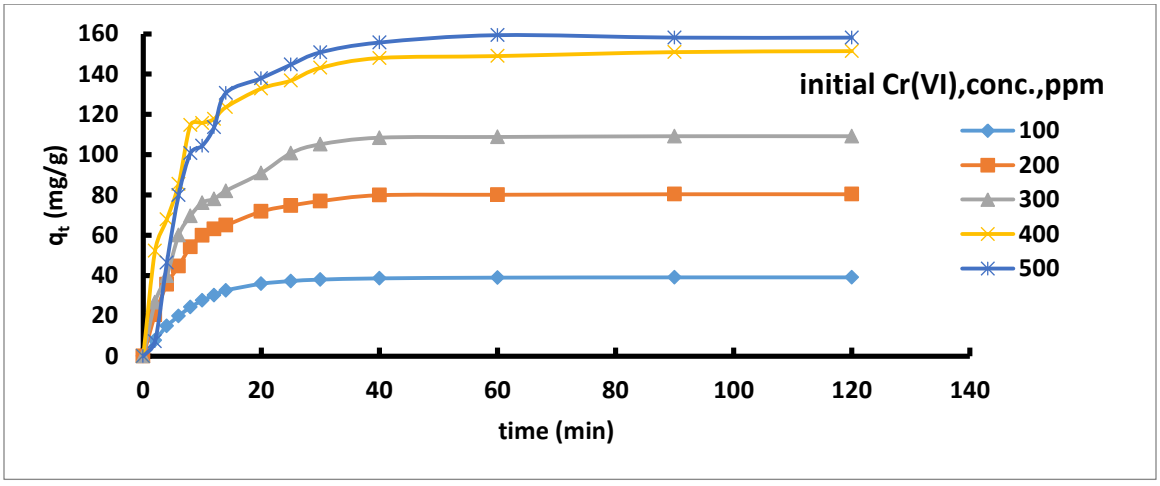

Figure 5-7 Ion exchange capacity versus time at different initial Cr(VI) conc. (pH of 4.28; Contact time of 120 min; amount of resin of 5 g; 350 rpm and Temp. 25±2 ^oC.)

5.1.2. **Equilibrium Studies:**

The sorption of Cr(VI) ions was carried out at different initial chromium concentrations at optimum pH . Sorption isotherms can be used to describe how solutes interact with the resin at equilibrium. Three kinds of known isotherm equations, Langmuir, Freundlich and Temkin

isotherms, have been applied for present study. These isotherms relate metal uptake per unit weight of resin q_e at equilibrium to the equilibrium metal ion concentration in the bulk fluid phase C_e. The three isotherms will be described in the following sections.

Langmuir Isotherm can be described by the following equation:

$$q_e = \frac{q_m K_L C_e}{1 + K_L C_e} \qquad (5.3)$$

Which in linearized form can be represented by the following equation:

$$\frac{C_e}{q_e} = \frac{1}{K_L q_m} + \frac{C_e}{q_m} \qquad (5.4)$$

Figure (5.8) represents the relation between C_e/q_e versus C_e using the present equilibrium data.
It is well seen that the present equilibrium data well fit the Langmuir isotherm with a high correlation coefficient (0.9987). This may indicate that sorption of Cr(VI) ions form mono adsorption layer on the resin. The present results are in agreement with other investigators.[33-38].

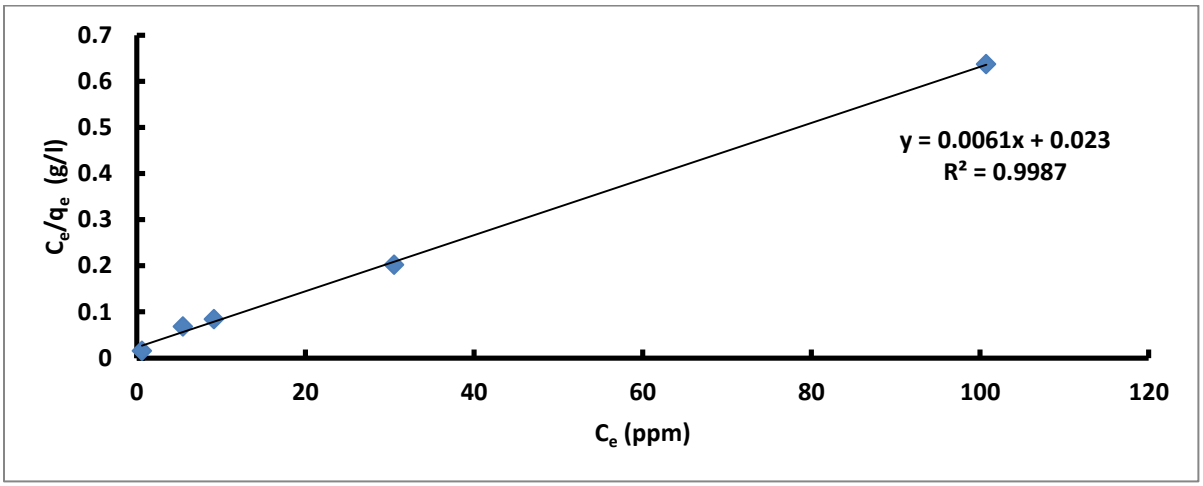

Figure 5-8 Langmuir isotherm of Cr(VI) sorption on Diaion SA20A (conditions: C_o = 100 - 500 ppm ; amount of resin, 5 g; temperature, 25±2 °C; stirring rate 350 rpm; stirring time: 120 min)

A separation factor (R_L) is a dimensionless constant, which can be represented by the following equation:

$$R_L = \frac{1}{1 + K_L C_o} \qquad (5.5)$$

Where K_L is the Langmuir constant and C_o is initial concentration. In a deeper explanation, R_L value indicates the adsorption nature to be either unfavorable ($R_L > 1$), linear ($R_L = 1$), favorable ($0 < R_L < 1$) or irreversible ($R_L = 0$).

Figure (5.9) depicts the relation of R_L versus initial Cr^{+6} conc. It is well obvious that values of R_L lay between 0 and 1 which indicate favorable sorption.

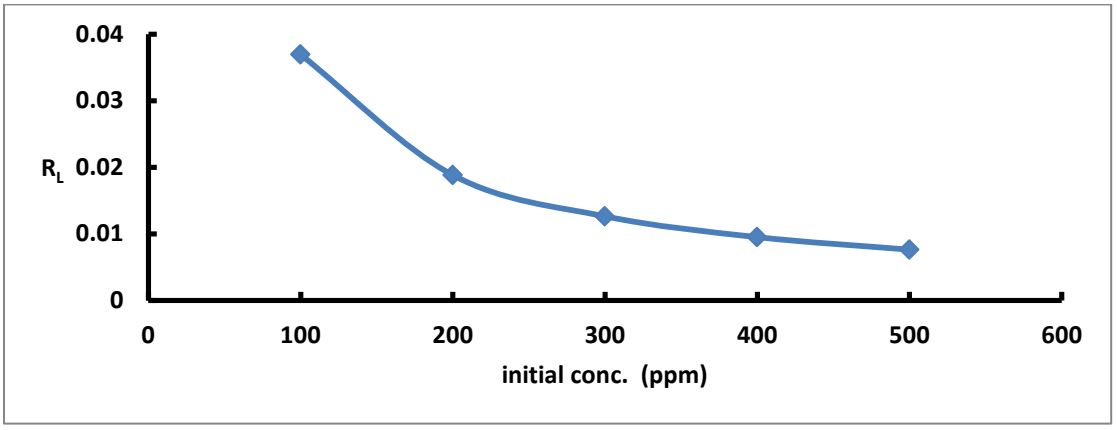

Figure 5-9 Separation factor of Cr (VI) sorption by ion exchange resin (DiaionAS20A).

Freundlich Isotherm can be described by the following equation:

$$q_e = K_f C_e^{n} \qquad (5.6)$$

Linearization of the Eq. (5.6) would yield the following equation.

$$\ln q_e = \ln K_f + n \ln C_e \qquad (5.7)$$

Figure (5.10) represents the relation between ln q_e versus ln C_e using the present equilibrium data. It is well noticed that the present data fit the Freundlich isotherm to a relatively high correlation coefficient (0.9406). The present results are in agreement with other investigators. [35-38]. The values of n (0 - 1) where its values represent adsorption intensity or surface heterogeneity, as the value of (n → 0) the surface becomes more heterogeneous. [87]

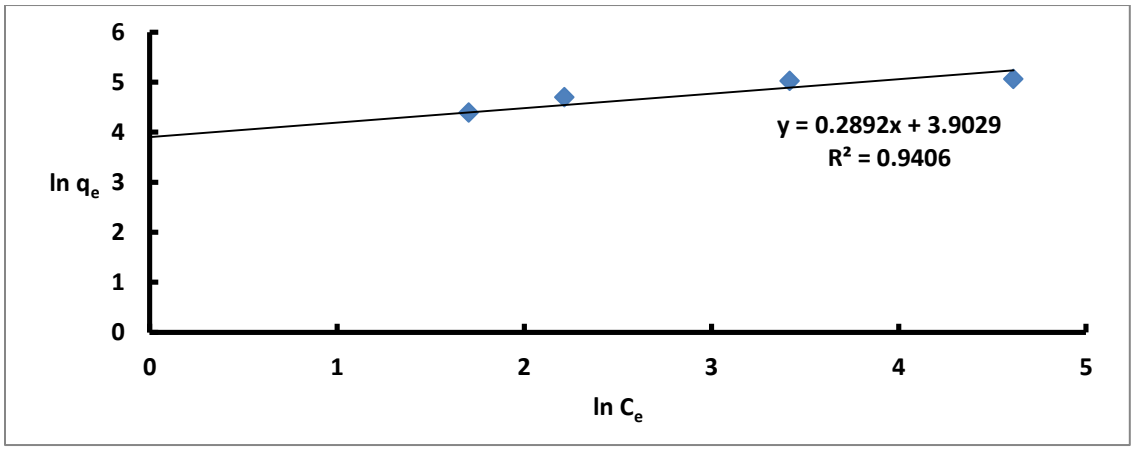

Figure 5-10 Freundlich isotherm of Cr(VI) sorption on Diaion SA20A (C_o =100 - 500 ppm ; amount of resin, 5 g; temp., 25±2 °C; stirring rate 350 rpm; stirring time, 120 min; pH,4.28)

Temkin Isotherm

The model could be represented by the following equations:

$$q_e = B \ln A_T + B \ln(C_e) \qquad (5.8)$$

$$\text{Where } B = \frac{RT}{b_T} \qquad (5.9)$$

Figure (5.11) shows the liner plots of q_e versus ln C_e of the present equilibrium data. The present data fit Temkin Isotherm to a relatively high extend. The results are in agreement with other investigators. [18, 41]

Table (5.1) gives the values of all constants of each isotherm with their correlation coefficient (R^2).

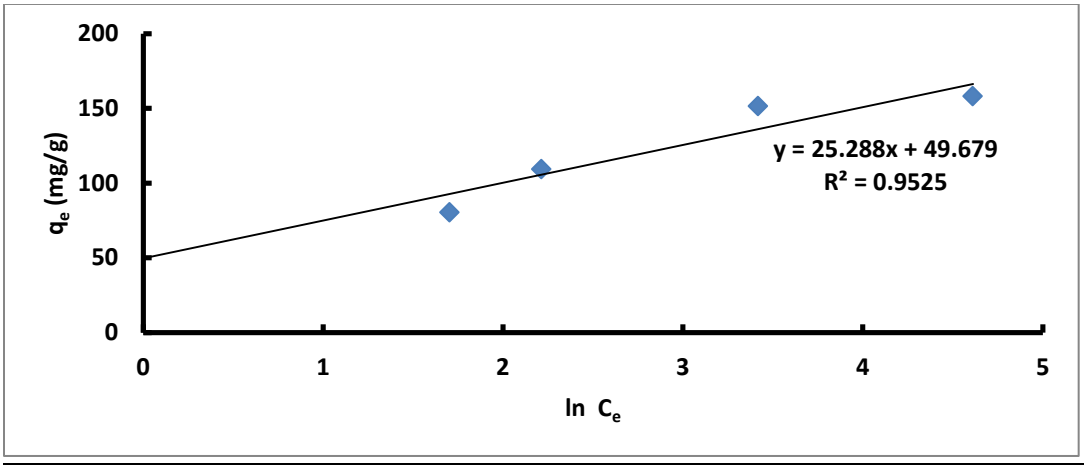

Figure 5-11 Temkin isotherm of Cr(VI) on Diaion SA20A (C_o = 100 -500 ppm ; amount of resin, 5 g; temp., 25±2 ◦C; stirring rate 350 rpm; stirring time, 120 min; initial pH, 4.28).

N.B. The equilibrium data were correlated with Langmuir isotherm indicating a monolayer adsorption on homogeneous active sites on the resin particles.

Table 5-1 Values of all constants of the investigated isotherms and their correlation coefficients.

Langmuir Model	**Freundlich Model**	**Temkin-isotherm-model**
q_m=166.6 mg/g K_L = 0.261 (l g^{-1}) R^2 = 0.9987	K_F = 49.501 (l g^{-1}) 1/n= 3.460 n = 0.289 R^2 = 0.9406	B = 25.28 (J/mol) b_T = 98.005 A_T=7.133 (lg^{-1}) R^2 = 0.9525
Error analysis	Error analysis	Error analysis
X^2 = 15.368 HYBRID = 11.400	X^2 = 10.069 HYBRID = 10.317	X^2 = 3.991 HYBRID = 4.085

5.1.3 **Kinetic studies:**

In order to investigate the mechanism of sorption and potential rate controlling steps such as mass transport and chemical reaction processes, kinetic models have been used to test the present experimental data. These kinetic models include the pseudo-first order model, the pseudo-second order model, Elovich kinetic model and intra-particle diffusion model.

The Pseudo-first Order Model:

The rate constant of adsorption can be determined from the following pseudo first-order rate:

$$\frac{dq_t}{dt} = k_1 (q_e - q_t) \qquad (5.10)$$

The integrated form of Eq. (5.10) becomes:

$$\log (q_e - q_t) = \log (q_e) - \left(\frac{k_1}{2.303}\right) t \qquad (5.11)$$

Figure (5.12) shows the relation between log (q_e-q_t) versus time at different initial Cr(VI) concentrations. The present data fit the pseudo-first order model with a high correlation coefficient. The driving force, (q_e−q_t), is proportional to the available fraction of active sites. [87] The pseudo-first order model proposed fits the experimental data well for an initial period of the first reaction step only. [88] Other investigators have found that sorption of Cr^{+6} in different ion exchangers to follow first order kinetics.[6,18,28,39]

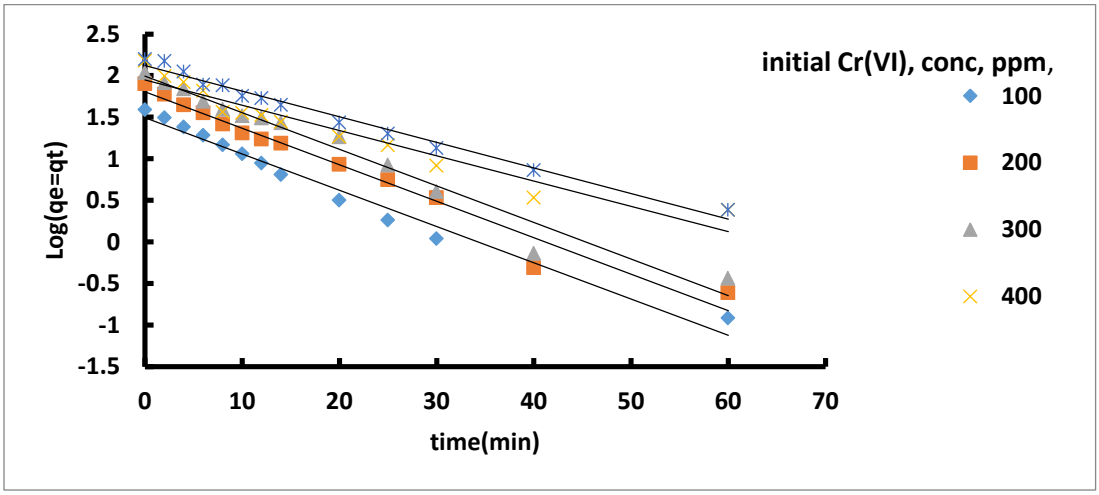

Figure 5-12 Pseudo-first order model for the adsorption of Cr(VI) onto (DiaionSA20A) , (amount of resin 5 g, pH 4.28, at 25±2 °C; time = 120 min. &350 rpm)

The Pseudo-second Order Model:

The rate constant of adsorption can be determined from the following pseudo second-order rate

$$\frac{t}{q_t} = \frac{1}{k_2 q_e^2} + \left(\frac{1}{q_e}\right) t \qquad (5.12)$$

$$h = k_2 q^2_e \qquad (5.13)$$

Where h can be regarded as the initial sorption rate as $q_t = 0$, $t = 0$.

Eq. (5.12) can be written as:

$$\frac{t}{q_t} = \frac{1}{h} + \left(\frac{1}{q_e}\right) t \qquad (5.14)$$

Figure (5.13) shows a plot of t/q_t versus t at different initial Cr(VI) concentrations. The present data fit to a great extend the pseudo-second order model with high correlation coefficient (0.99). This suggests that this sorption system is not a first order reaction and that the pseudo-second order model, based on the assumption that the rate-limiting step may be chemical sorption or

chemisorption involving valency forces through sharing or exchange of electrons between sorbent and sorbate, provides the best correlation of the data. [88]
The present trend is in agreement with previous studies. [31-39]

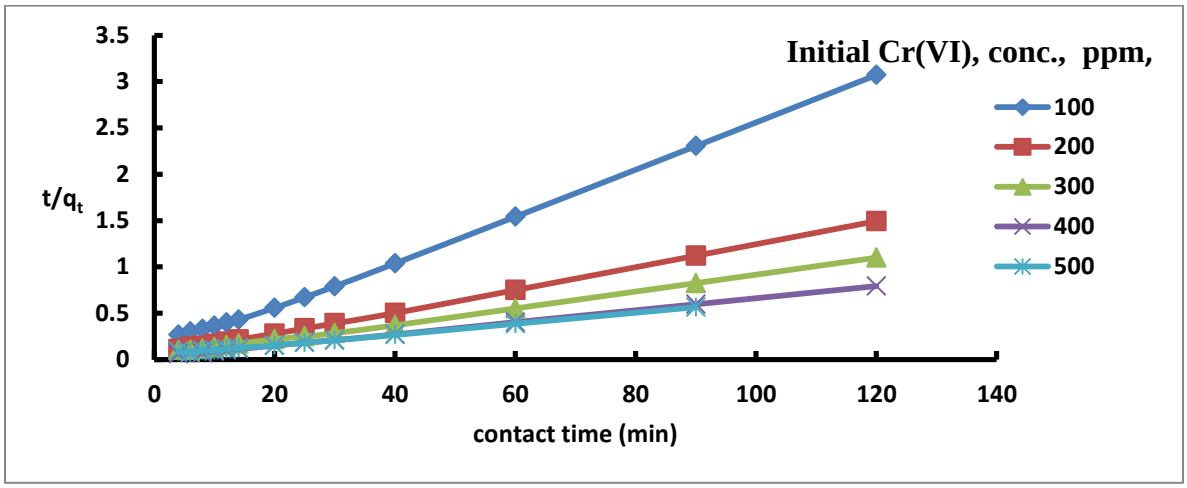

Figure 5-13 Pseudo-second-order kinetic plot for the adsorption of Cr(VI) onto (DiaionSA20A), (amount of resin 5 g ,pH 4.28, at 25±2 °C; time = 120 min. & 350 rpm)

Elovich Kinetic Model:
The linear form of Elovich Equation is given by the following equation:

$$q_t = \frac{\ln a_e b_e}{b_e} + \frac{1}{b_e} \ln t \qquad (5.15)$$

Fig. (5.14) represents a plot of q_t versus lnt at various initial Cr^{+6} conc., and table (5.2) lists the kinetic constants obtained from the Elovich equation.

It will be seen that the Elovich kinetic model fits the present kinetic data to a relatively good extend, particularly at low initial Cr^{+6} conc., however the model does not fit the kinetic data at initial conc. greater than 300 ppm.

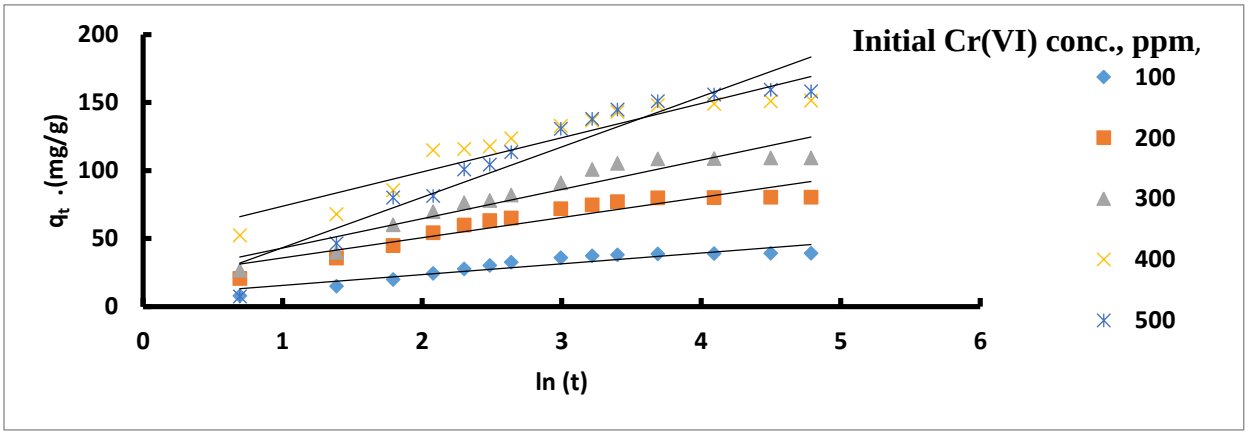

Figure 5-14 Elovich kinetic plot for ion exchange of Cr (VI) onto (DiaionSA20A), (resin dose = 5 g, pH 4.28, at 25±2 °C; time =120 min. & 350 rpm)

Intra-particle Diffusion Model:

The intra-particle diffusion model is represented by the following equation:

$$q_t = k_i t^{1/2} + c \qquad (5.16)$$

Figure (5.15) shows the relation between q_t versus $t^{0.5}$ at different initial Cr(VI)conc. and Figure (5.16) represents intra-particle diffusion model. The results revealed that both film diffusion and intraparticle diffusion contribute to the rate- determining steps. The present results are in agreement with other investigators. [32,33,35,36]

It is obvious that at conc. = 500ppm, the contribution of external film diffusion is negligible i.e. the reaction is mainly controlled by intraparticle diffusion.

Table (5.2) gives a summary of the values of parameters of all investigated models and their correlation coefficients.

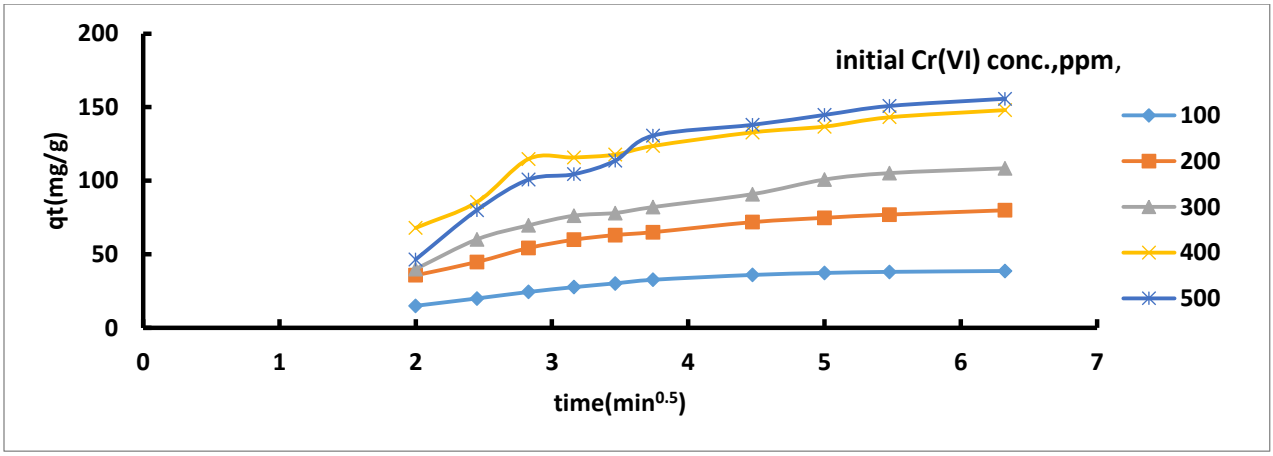

Figure 5-15 q_t versus $t^{0.5}$ at different initial Cr(VI)conc. for ion exchange of Cr (VI) onto (DiaionSA20A), (resin dose 5 g, pH 4.28, at 25±2C° time =120min. & 350 rpm)

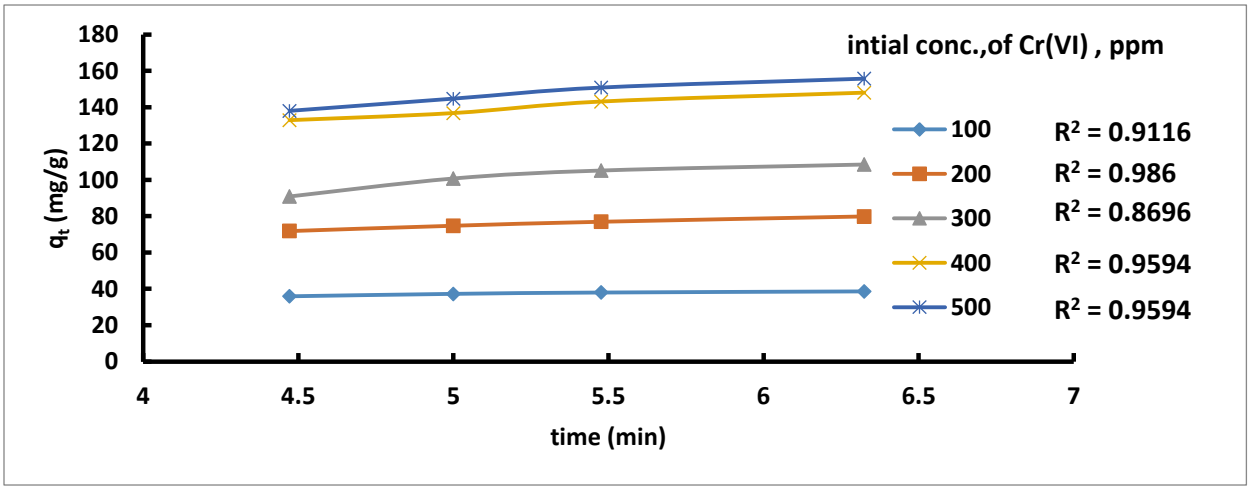

Figure 5-16 intra-particle diffusion model plot for the sorption of Cr (VI) onto (DiaionSA20A), (resin dose 5 g, pH 4.28, at 25±2 C° time =120min. & 350 rpm)

N.B. The kinetic study shows that sorption of Cr(VI) on the studied resin follows the pseudo-second order equation and is controlled by film diffusion in the initial stage and by intraparticale diffusion in later stage.

The following observations were concluded from table (5-2):

- Pseudo –first order (k_1) increases with increasing the initial conc., but the model does not fit the kinetic data at initial conc. greater than 300 ppm.
- Pseudo- second order (k_2) decreases with increasing the initial conc.,(100-300ppm) while the initial rate (h) increasing except at C_o =500ppm. Error analysis =1.9 compared to experimental data.
- Elovich kinetics model, the initial adsorption rate (a_e) increases with the increase of C_o except at C_o= 500ppm.
- Intra particle model (k_i) increases with the increase of the initial concentration.

Table 5-2 Kinetic model parameters for Cr (VI) sorption on Diaion SA20A.

Pseudo –first order			**Pseudo- second order**			
C_o(ppm)	k_1 (min^{-1})	R^2	C_o (ppm)	k_2(g mg^{-1} min^{-1})	h(mg/(g.min))	R^2
100	0.1004108	0.9809	100	0.0048	8.474	0.997
200	0.1011017	0.9718	200	0.0024	20.408	0.998
300	0.101332	0.9694	300	0.0014	22.222	0.998
400	0.0700112	0.9316	400	0.0015	41.666	0.999
500	0.0709324	0.9841	500	0.0004	14.492	0.918
%SSE	=5.090		%SSE	=1.901		
Intra-particle diffusion model				**Elovich kinetics model**		
C_o(ppm)	k_i (mg $g^{-1}min^{1/2}$)	C	R^2	C_o (ppm)	b_e	a_e	R^2
100	1.4038	29.957	0.9116	100	0.126	20.506	0.86
200	4.3061	52.922	0.986	200	0.067	60.382	0.878
300	9.06	53.097	0.8696	300	0.046	58.443	0.904
400	8.4179	95.4	0.9737	400	0.039	173.835	0.879
500	9.5458	96.514	0.9594	500	0.027	43.848	0.912
%SSE	= 12.3055			%SSE	= 2.6492		

5.2. **Column Study:**

5.2.1. **Column Data Analysis:** [3]

The time for breakthrough, appearance and the shape of the breakthrough curve are very important characteristics for determining the operation and dynamic response of a sorption column. The effluent concentration (C_t) from the column that reaches about 0.1% of the influent concentration (C_0) conc. is taken as breakthrough point. The point where the effluent concentration reaches 95% is taken as the ‘‘point of column exhaustion’’. The breakthrough curve is usually expressed by C_t/C_0 as a function of time or treated volume of the effluent for a given bed depth. The effluent volume, V_{eff}, can be calculated from the following equation:

$$V_{eff} = Qt_{total} \qquad (5.17)$$

Where Q is the volumetric flow rate, t_{total} is the total flow time.

The value of the total mass of metal adsorbed, q_{total} (mg) can be calculated from the area under the breakthrough curve according to the following equation:

$$q_{total} = \frac{Q}{1000} \int_{t=0}^{t=total} C_{ad}\, dt \qquad (5.18)$$

Where C_{ad} is the concentration of metal removed (mg/l), the area under the curve can be obtained by plotting C_{ad} versus time.

Equilibrium metal uptake or maximum capacity of the column, q_{eq} (mg/g), in the column is calculated as the following:

$$q_{eq} = \frac{q_{total}}{w} \qquad (5.19)$$

Where w is the dry weight of adsorbent in the column (g).Total amount of metal ion entering column (m_{total}) is calculated from the following equation:

$$m_{total} = \frac{C_o Q t_{total}}{1000} \qquad (5.20)$$

And the removal percentage of Cr(VI) ions can be obtained from Eq. (5.21).

$$Y(\%) = \frac{q_{total}}{m_{total}} \times 100 \qquad (5.21)$$

(EBCT) in the column, can be described by the following equation:

$$EBCT = \frac{\text{bed volume}}{\text{volumetric flow rate}} \qquad (5.22)$$

Table (5.3), shows the calculations of the previous terms at different bed height and flow rate.

Table 5-3 Summary of the fixed bed terms calculations at different bed heights and flow rates.

Q	w	Z	C_o	t_{total}	m_{total}	q_{total}	q_{eq}	V_{eff}	Y	EBCT
(ml/min)	(g)	(cm)	(ppm)	(min)	(mg)	(mg)	(mg/g)	(ml)	(%)	(min)
	different heights									
60	2.5	4	490	55	1617	97.778	39.1112	3300	6.0469	0.0633
60	5	7	490	70	2058	815.761	163.152	4200	39.639	0.1108
60	7.5	12	490	85	2499	1297.512	173.002	5100	51.921	0.19
20	10	16	542	460	4986.4	1532.181	153.218	9200	30.727	0.7599
35	5	7	495	140	2425.5	625.447	125.089	4900	25.786	0.19
45	5	7	578	120	3121.2	1354.485	270.897	5400	43.396	0.1478
48	5	7	519	80	1992.96	1177.718	235.544	3840	59.094	0.1385
68	5	7	499	105	3562.86	1266.684	253.337	7140	35.552	0.0978
95	5	7	504	40	1915.2	777.055	155.411	3800	40.573	0.07
48	7.5	12	499	190	4550.88	2982.236	397.631	9120	65.531	0.2375
60	7.5	12	490	85	2499	1277.866	170.382	5100	51.135	0.19

As shown in Table (5.3), the bed depth strongly influenced the Cr(VI) uptake capacity as it increases from 39 to173 mg/g corresponding to an increase of bed depth from 4 to 12 cm,

respectively. The increase in Cr(VI) uptake capacity with the increasing bed depth in the fixed-bed column may be due to increased adsorbent surface area, which provided more binding sites for the column adsorption.[3]
A longer exhaustion time was observed in Table (5.3), when the bed depth was increased to 12 cm. The EBCT also increased from 0.063 to 0.1899 min with the bed depth increasing from 4 to 12 cm, also Table (5.3) shows that V_{eff} increases from 3300 to 5100(ml) with the increase of bed height from 4 to 12 cm.

5.2.2. **Effect of Different Bed Depths on Breakthrough Curve**:

Figure (5.17) shows a plot of breakthrough curves at different bed heights. It is very clear that as the bed depth increases, breakthrough time and the exhaustion time increases. It is also well noticed that as the bed height decreases, the slopes of breakthrough become sharper. A broaden of MTZ with the increase of bed height indicates that as the bed height increases, resistance to mass transfer increases. It is obvious that %removal increases with increasing bed depth. The present trends are in agreement with other investigators. [3,86]

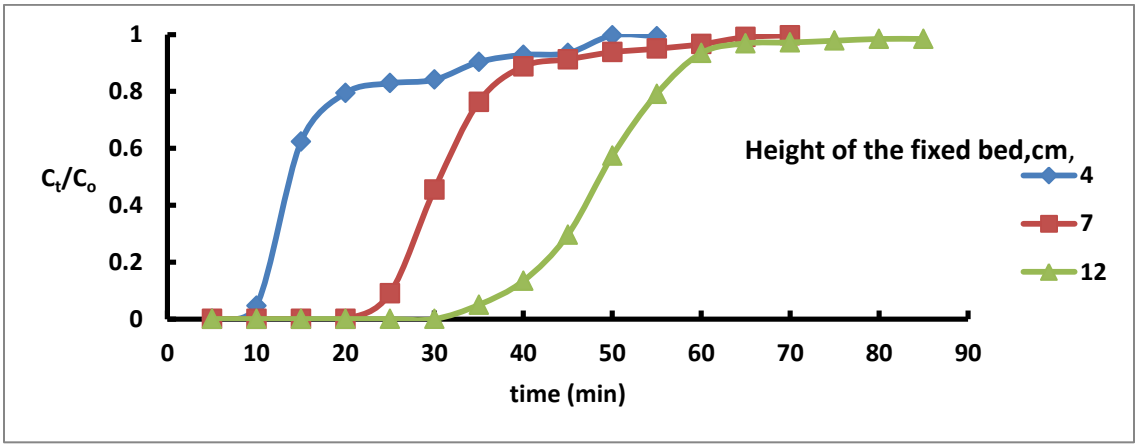

Figure 5-17 shows a plot of breakthrough curves of Cr(VI) adsorption on Diaion SA20A at different bed heights. (Conditions :C_o = 500 ppm; flow rate = 60 mL/min; pH =4.28 & temp. = 25±2 C^o)]

5.2.3. **Effect of Flow Rate on Breakthrough Curve**:

Figure (5.18) shows a plot of breakthrough curves at different flow rates. It is well noted that the breakthrough occurs significantly faster with increasing flow rate with steeper slopes of breakthrough curves.
This behavior may be attributed to that at higher flow rate, the external film mass transfer resistance tends to decease, which results in short MTZ, and steeper breakthrough curve. [3, 73]

In Fig. (5.18). As it can be seen from the breakthrough plots, higher efficiency of the process was achieved at lower flow rate, the diffusion process which controls the sorption becomes slow, and hence, the sorbent needs more time to bond the metals efficiently.
At higher flow rates breakthrough curves become steeper and breakpoint time and the adsorbed ion concentration decreases. A higher uptake of chromium was observed at the beginning of fixed bed column operation but as solution continued to flow, the concentration of chromium in the effluent rapidly increased; the bed becomes saturated with chromium and the concentration of the solute in the effluent rise sharply. [86]

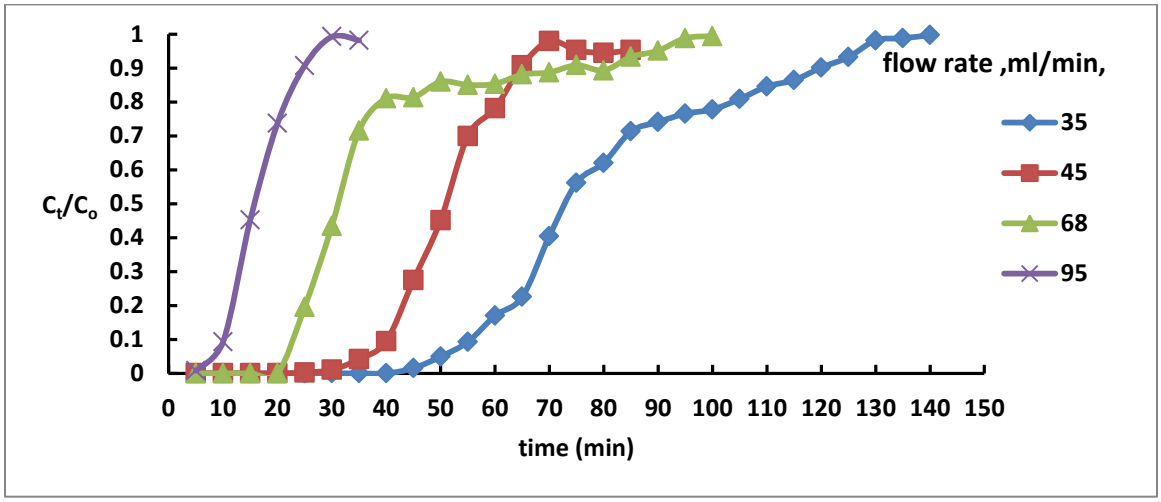

Figure 5-18 shows a plot of breakthrough curve of Cr(VI) adsorption on Diaion SA20A at different flow rates. (bed depth 7 cm; C_o = 500 ppm; pH =4.28 & temp.= 25±2 C^o.)

5.2.4. **Breakthrough Curve Modeling:**

Successful design of an ion exchange column requires prediction of the breakthrough curve for the effluent. Over the years, several simple mathematical models have been examined for describing and analyzing the lab-scale column studies for the purpose of industrial applications. Thus in the present study, the Adams–Bohart, Thomas and Yoon-Nelson models were investigated to identify the best model for predicting the dynamic behavior of the column.

Adams–Bohart Model:

This model can be expressed according to the following equation:

$$\ln\left(\frac{C_t}{C_o}\right) = k_{AB}C_o t - k_{AB}N_o\left(\frac{Z}{U_o}\right) \qquad (5.23)$$

Figure (5.19) represents a typical plot of $\ln(C_t/C_o)$ versus t, the values of k_{AB} and N_0 parameters of Adams–Bohart model were determined from the slope and intercept of the curve respectively. For all breakthrough curves using linear regression analysis, respective values of k_{AB} and N_0 were calculated and presented in Table (5.4), along with the correlation coefficients (R^2).

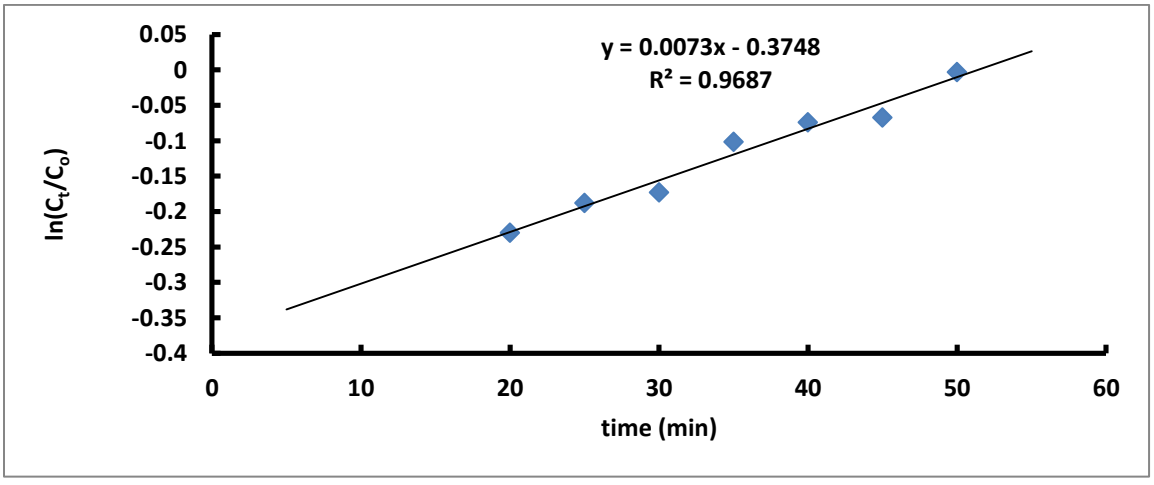

Figure 5-19 A typical curve for Adams–Bohart Model (Conditions: Diaion SA20A resin = 2.5g; bed depth 4 cm; C_o = 500 ppm; pH =4.28 & temp. = 25±2 C^o.

Table 5-4 Parameters of Adams–Bohart model under different conditions using linear regression analysis:

C_o	Q	Z	w	pH	Adam-Bohart		
(ppm)	(ml/min)	(cm)	(g)		$K_{AB}x10^{-4}$	N_o	R^2
different heights					(l/mg min)	(mg/l)	
490	60	4	2.5	4.28	0.14898	397088	0.9687
490	60	7	5	4.28	0.07959	301100.2	0.9792
490	60	12	7.5	4.28	2.408	148239	0.9339
542	20	16	10	4.28	0.01476	3264.6435	0.9901
495	35	7	5	4.28	0.1616	34905.8	0.9353
578	45	7	5	4.28	2.84	241475.5	0.9344
519	48	7	5	4.28	0.331407	306903	0.9577
499	68	7	5	4.28	0.066	559886.5	0.9497
504	95	7	5	4.28	1.33	480723.6	0.8541
499	48	12	7.5	4.28	0.89	379784.6	0.9473
490	60	12	7.5	4.28	2.408	148239	0.9339

Thomas Model:

The linearized form of this model can be described by the following expression:

$$\ln\left(\frac{C_o}{C_t} - 1\right) = \frac{k_{Th}q_o w}{Q} - k_{Th}C_o t \qquad (5.24)$$

Figure (5.20) represents a typical plot of $\ln((C_o/C_t)-1)$ versus t, the values of k_{Th} and q_o parameters of Thomas Model were determined from the slope and the intercept of the curve respectively.

The relative constants and coefficients were obtained using linear regression analysis according to Eq. (5.24) and the results were presented in Table (5.5). It can be seen that with the bed depth increasing, the k_{Th} and q_o values increased. In case of height 12cm, flow rates 48 &60 (ml/min), as the flow rate increased, the value of k_{Th} increased while the value of q_0 decreased. Thus the lower flow rate and higher bed depth would increase the adsorption of Cr(VI) on the column.

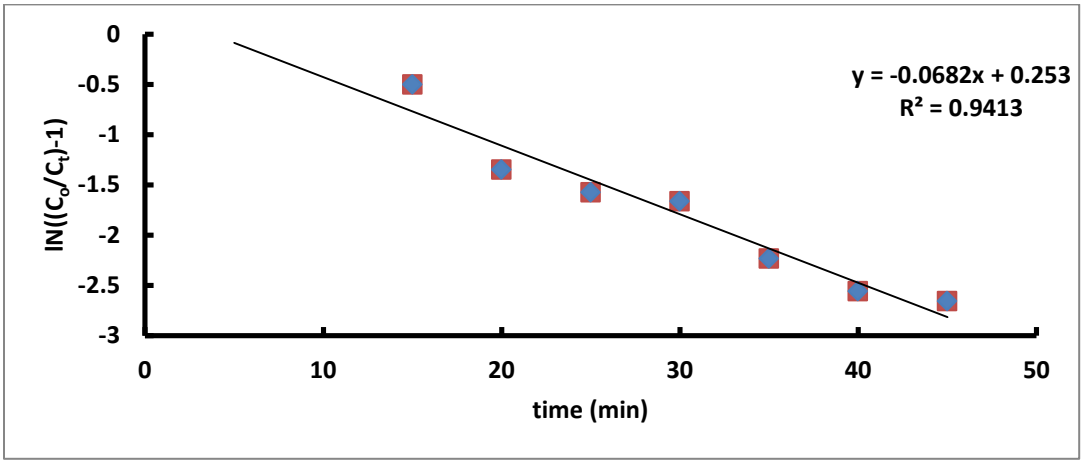

Figure 5-20 A typical curve for Thomas Model (Conditions: Diaion SA20A resin = 2.5g; bed depth= 4 cm; C_o = 500 ppm; pH =4.28 & temp. = 25±2 C°.)

Table 5-5 Parameters of Thomas model under different conditions using linear regression analysis and standard error results.

C_o	Q	Z	w	pH	Thomas model			
(ppm)	(ml/min)	(cm)	(g)		$K_{Th}x10^{-4}$	q_o	R^2	SE
different heights					(ml/mg min)	(mg/g)		
490	60	4	2.5	4.28	1.39	43.683	0.9413	1.378
490	60	7	5	4.28	2.54	164.244	0.9382	0.471
490	60	12	7.5	4.28	3.37	193.457	0.9457	5.596
542	20	16	10	4.28	0.26384	186.332	0.9887	3.433
495	35	7	5	4.28	1.448	280.705	0.9407	29.408
578	45	7	5	4.28	2.3235	327.672	0.9098	13.769
519	48	7	5	4.28	3.036	260.774	0.9606	6.307
499	68	7	5	4.28	1.34	242.252	0.8845	2.418
504	95	7	5	4.28	2	146.404	0.9193	3.184
499	48	12	7.5	4.28	1.874	462.275	0.982	10.486
490	60	12	7.5	4.28	3.37	193.457	0.9457	5.596

Yoon–Nelson Model:

The linearized Yoon–Nelson model for a single component system can be expressed as follows:

$$\ln\left(\frac{C_t}{C_o - C_t}\right) = k_{YN}t - k_{YN}\tau \qquad (5.25)$$

Figure (5.21) represents a typical plot of $\ln(C_t/(C_o-C_t))$ versus t, the values of k_{YN} and τ parameters of Yoon –Nelson model were determined from the slop and intercept of the curve respectively.

Different statistical parameters of the Yoon–Nelson model were calculated and given in Table (5.6). The R^2 values indicated the validity of Yoon–Nelson model for the present system. In a comparison of values of R^2, both the Thomas and Yoon–Nelson models can be used to predict breakthrough curves for adsorption of Cr(VI) in a fixed-bed column. The k_{YN} values and the 50% breakthrough time τ both increased with increasing bed depth.

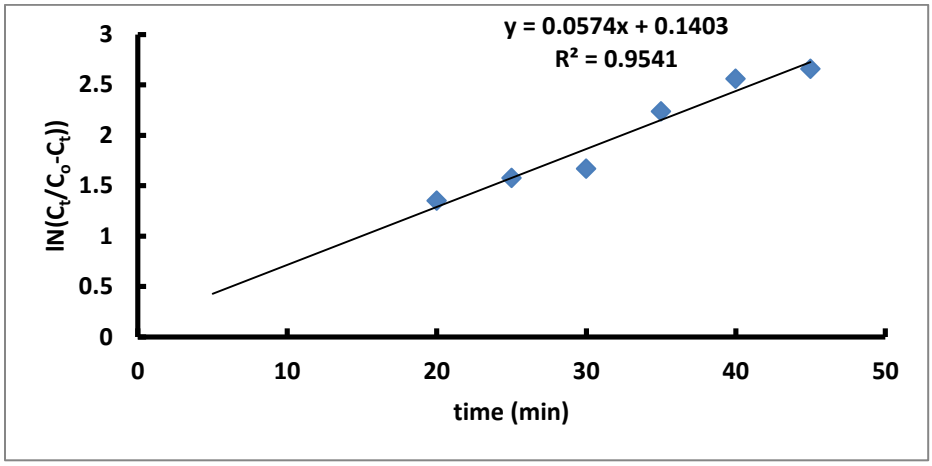

Figure 5-21 A typical curve for Yoon–Nelson Model (Conditions: Diaion SA20A resin = 2.5g; bed depth 4 cm; C_o = 500 mg/L; pH =4.28 & temp.= 25±2 C°.)

Table 5-6 Parameters of Yoon–Nelson model under different conditions using linear regression analysis and standard error results.

C_o	Q	Z	w	pH	Yoon-Nelson			
(ppm)	(ml/min)	(cm)	(g)		K_{YN}	τ	R^2	SE
different heights					(min^{-1})	(min)		
490	60	4	2.5	4.28	0.0574	2.444	0.9541	3.126
490	60	7	5	4.28	0.1247	27.578	0.9382	0.086
490	60	12	7.5	4.28	0.1651	49.306	0.9454	5.553
542	20	16	10	4.28	0.0135	162.925	0.9846	2.425
495	35	5	7	4.28	0.0673	75.484	0.873	25.789
578	45	5	7	4.28	0.1125	60.682	0.9504	10.858
519	48	5	7	4.28	0.1527	53.814	0.9631	8.145
499	68	5	7	4.28	0.0588	34.376	0.8265	4.374
504	95	5	7	4.28	0.2008	24.675	0.9119	28.596
499	48	7.5	12	4.28	0.0853	137.0809	0.9448	6.513
490	60	7.5	12	4.28	0.1651	49.306	0.9454	5.553

5.2.5. **Bed Depth Service Time (BDST) model**:

The Bed Depth Service Time (BDST) model equation can be expressed as.

$$t_b = \frac{N_o Z}{C_o V} - \frac{1}{K\ C_o} \ln\left(\frac{C_o}{C_b} - 1\right) \qquad (5.26)$$

Fig.(5.17) shows the breakthrough curves of Cr(IV) adsorption onto DnionSA20A at different bed depths (4, 7 and 12 cm) t_b were taken at (C_t/C_o) =0.93. The plot of service time against bed height at a flow rate of 60 ml/min (Fig.5.22) was linear (R^2 = 0.9978), indicating the validity of BDST model for the present system. The computed N_0 is 3505899.982 mg/l. The BDST model parameters can be useful to scale up the process for other flow rates without further experiments.

Table 5-8 represents BDST calculated time

Table 5-7 Bed Depth Service Time (BDST) model

Z cm	t_b (min)	flow rate (ml/min)	BDST(min)
4	45	60	47.756
7	50	60	57.195
12	60	60	76.073

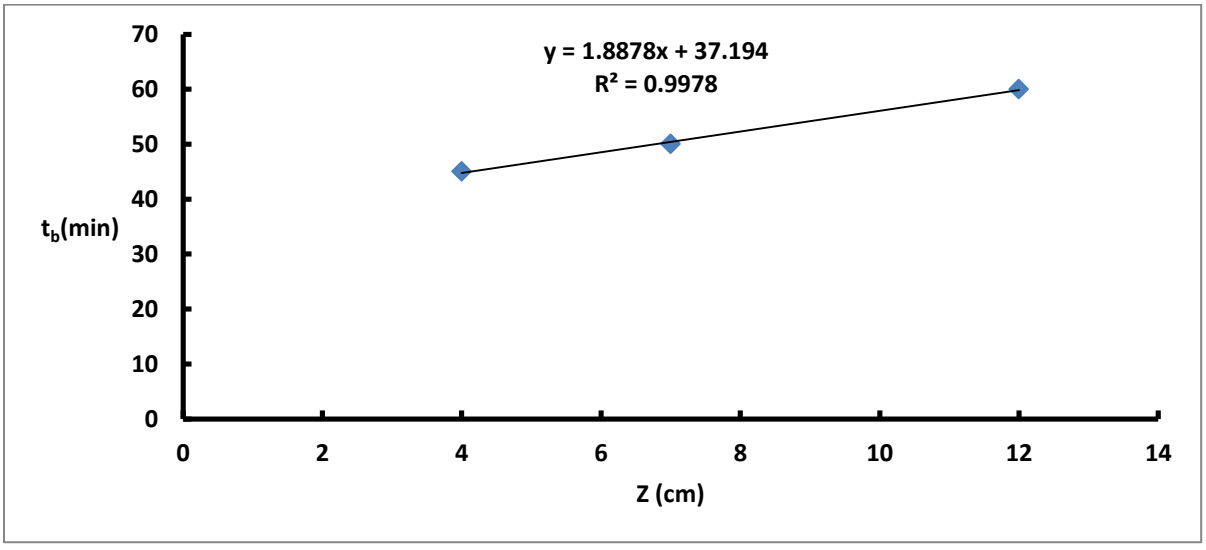

Figure 5-22 The BDST Model of Cr(VI) on (a) Diaion SA20A (conditions: initial concentration of Cr(VI), 500 ppm ; bed depth (4,7,12 cm); temperature, 25±2 ˚C; flow rate 60 ml/min; initial pH, 4.28)